JOURNAL OF COMPUTATIONAL PHYSICS 69, 175–195 (1987)

Simple Adaptive Grids for 1-D Initial Value Problems

E. A. DORFI* AND L. O'C. DRURY†

Max-Planck-Institut für Kernphysik, Postfach 103980, D-6900 Heidelberg, Federal Republic of Germany

Received April 8, 1985; revised April 11, 1986

In solving 1-D initial value problems by implicit finite difference methods it is advantageous to use an adaptive grid to provide local regions of high resolution and allow larger time steps to be taken. A simple method of constructing such grids is presented and the benefits are demonstrated by calculations of Sod's shock tube problem (G. A. Sod, *J. Comput. Phys.* **27**, 1 (1978)) and of a supernova explosion.

1. INTRODUCTION

Most astrophysical flows, even when they only involve pure gas dynamics in one spatial dimension, are complicated to compute because many orders of magnitude have to be covered in the time and space evolution. Of course this problem is not confined to Astrophysics, but it is here particularly acute and has stimulated the development of a promising method which at least partially solves the problem, the implicit adaptive mesh technique [14, 16, 17, 18]. Here a fixed number of grid-points is redistributed during the evolution to optimize the resolution of developing and moving flow features. The system of physical equations is extended by adjoining an additional "grid equation" which specifies the spatial distribution of the grid-points. The augmented system is then solved simultaneously using an implicit method to avoid the very short time steps which the Courant–Friedrichs–Lewy stability condition [3] would require if an explicit method were used.

This simultaneous solution of the physical equations and the grid equation should be contrasted with methods in which the physical equations are advanced on a fixed grid and the calculation is interrupted at regular intervals for grid rezoning [5, 6]. The solution at the rezoned gridpoints has then to be constructed by some interpolation algorithm. On the other hand methods which use an explicitly specified transformation of the spatial coordinate system [15] may run into

* Present address: Institut für Astronomie der Universität Wien, Türkenschanzstrasse 17, A-1180 Vienna, Austria.

†Present address: Dublin Institute for Advanced Studies, School of Cosmic Physics, Cosmic Ray Section, 5 Merrion Square, Dublin 2, Ireland.

0021-9991/87 $3.00

581/69/1-12

problems if the character of the solution changes from continuous to discontinuous and in an implicit scheme require the inversion of full rather than band matrices. An alternative solution to the problem of resolving large gradients is given in [11]; there, by applying the method of lines, a system of PDEs is converted to ODEs and then the equations are mapped through an analytical transformation from the physical space to the computational space. Powerful methods have been developed in constructing multidimensional adaptive grids [2, 7] by choosing one variable to determine the mapping from the physical into the computational mesh, but for the astrophysical applications we have in mind we need to resolve large gradients in many different physical quantities (e.g., density, pressure, opacity, chemical composition, etc.). The moving finite element methods [5, 8] look quite promising but to our knowledge no results showing high grid refinements in the context of complicated interacting shock structures have been obtained with these methods. It is important to test numerical methods on difficult problems and we regard the "supernova explosion" presented in the last section as a suitable touchstone for evaluating adaptive grid methods.

The chief practical difficulty facing the method is that of formulating a satisfactory grid equation. It should be capable of handling problems with multiple variables each varying over many orders of magnitude, it should have the same numerical character as the dynamical equations (e.g., 5 point in space and 2 point in time), it should be capable of producing grids which are locally compressed by factors of at least 10^4 when compared with uniform grids, and finally it should be computationally efficient (e.g., vectorizable) and easy to program. Unlike the problem of discretizing the physical equations this task is purely artificial; thus we cannot be guided by physical arguments and must instead rely on numerical principles and a careful analysis of what the equation should do. This leads not to a single grid equation, but rather to a general method of constructing an equation adapted to the specific problem being studied. While our method is certainly not the only way of solving the problem it does appear to be simple and robust. Although not free of adjustable parameters we have never had to "fine-tune" them and have never produced unphysical grids.

2. Construction of a Grid Equation

Let us consider an initial value problem for a system of partial differential equations with two independent variables, a spatial variable x and a time variable t. We discretize the solution at N grid points, $x_1,..., x_N$, which we wish to distribute during the evolution in such a way that the solution is uniformly resolved; where high resolution is required, e.g., where steep gradients occur, the points should be concentrated and where lower spatial resolution suffices the points should be spread out. Our basic idea is to define measures of these two aspects, the point concentration n (which one can think of as the attained resolution), and the desired resolution R, and then distribute the points so that n is proportional to R, the con-

stant of proportionality being determined by the total number of points and the separation of the bondaries. The fundamental form of our grid equation is thus

$$n \propto R. \tag{1}$$

However, because stability considerations usually require that the point concentration not change too rapidly in either space or time, we make n proportional not directly to R, but to the result of applying temporal and spatial smoothing operators to R.

The point concentration we define to be the number of grid points per length scale,

$$n_i = \frac{X}{x_{i+1} - x_i}, \tag{2}$$

where X is a natural length scale (which may be any smooth positive function of space and time) determined by the problem. In the absence of structure in the solution a default grid is defined by n constant. Thus if X is independent of x the default distribution will be uniform and if $X = x$ it will be logarithmic. More complicated default grids can easily be created by choosing appropriate definitions of X.

The desired resolution, R, is a more subjective quantity whose definition necessarily depends on the nature of the problem being solved, the numerical method being used and the personal bias of the investigator. It is obviously essential that R be positive definite, but apart from this it can be any smooth function of the solution and its derivatives. A simple prescription which we have found to give very satisfactory results is motivated by the idea that in the case of one function, f, the data points should be distributed uniformly in arc-length along the graph of f. This suggess $R = \sqrt{1 + (df/dx)^2}$ which we generalize to several functions, $f_1, \ldots, f_M$, and discretize in the form

$$R_i = \left(1 + \sum_{j=1}^{M} \left(\frac{X_i}{F_j} \frac{f_{j,i+1} - f_{j,i}}{x_{i+1} - x_i}\right)^2\right)^{1/2}, \tag{3}$$

where F_j is a natural scale associated with the function f_j and $f_{j,i} = f_j(x_i)$. However, note that unlike [15] we do not transform to an "arc-length" coordinate. For artificial problems where all variables are of order unity one can of course set all scales X_i, F_j to unity; however in physical applications they are required on dimensional grounds alone.

It is perhaps worth noting that R_i must be obtained by discretizing some function R. This ensures that the only slight dependence of R_i on the grid point distribution comes from the inevitable discretization error. Clearly the required resolution is an intrinsic property of the problem and its solution which should not depend on the actual grid.

Our choice of spatial smoothing is based on the well-known rule of thumb, that

for stability the grid spacing should not change from one interval to the next by more than about 20 or 30%. We interpret this as the requirement

$$\frac{\alpha}{\alpha+1} \leqslant \frac{n_{i+1}}{n_i} \leqslant \frac{\alpha+1}{\alpha}, \tag{4}$$

where α is a measure of the grid "rigidity." The simplest way to achieve this, bearing in mind that R is positive definite, is to smooth the right-hand side of Eq. (1) and write

$$n_i \propto \sum_j R_j \left(\frac{\alpha}{\alpha+1}\right)^{|i-j|}, \tag{5}$$

but this smoothing kernel (neglecting for the moment the question of the boundary conditions) is the Green's function associated with the difference operator

$$1-\alpha(\alpha+1)\,\delta^2, \tag{6}$$

where δ denotes a centred difference. Thus we can replace the smoothing on the right by a differencing on the left and write

$$\tilde{n}_i = n_i - \alpha(\alpha+1)(n_{i+1} - 2n_i + n_{i-1}) \propto R_i. \tag{7}$$

Actually as boundary conditions for the grid equation we set the concentration gradient to zero,

$$n_1 = n_2, \qquad n_{N-2} = n_{N-1} \tag{8}$$

so that the true Green's function is slightly more complicated, but the difference is imperceptible except near a boundary.

To smooth the time dependence we use a similar idea, in effect replacing $R(t)$ by

$$\int_0^\infty R(t-t')\exp(-t'/\tau)\,dt'/\tau. \tag{9}$$

To achieve this we write equation in the form

$$\hat{n}_i = \tilde{n}_i + \frac{\tau}{\Delta t}(\tilde{n}_i - \tilde{n}_i^{(\mathrm{old})}) \propto R_i, \tag{10}$$

where Δt is the time step. The grid then adjusts on a time-scale τ and ignores variations on shorter time-scales. As with the other scales, τ can be a constant, or vary in some smooth fashion appropriate to the problem.

Finally we eliminate the constant of proportionality and obtain the grid equation,

$$\frac{\hat{n}_{i-1}}{R_{i-1}} = \frac{\hat{n}_i}{R_i}, \tag{11}$$

where $\hat{n}$ is defined by Eqs. (10), (7), and (2). (We note in passing that the other two obvious ways of writing this equation, $\hat{n}_i R_{i-1} = \hat{n}_{i-1} R_i$ and $R_i/\hat{n}_i = R_{i-1}/\hat{n}_{i-1}$, do not appear to function as well numerically in simple tests; when the grid was adjusting rapidly roughly twice as many time steps had to be taken, however, in practical applications the time step is normally controlled by the physical equations so that there should be no significant difference.) The left-hand side of the equation is 5-point in space and 2-level in time. Without increasing the complexity R can be any smooth function of the solution, its first three spatial derivatives and its first time derivative.

An important aspect of this equation is that with n and R regarded as indeterminate quantities it is summable, i.e., the general solution of the difference equation can be written down by reversing the steps taken above. This discrete analog of integrability is a nontrivial property and expresses mathematically the separation we have enforced between the problem of defining what the grid should do (the measures of the attained and desired resolution, n and R) and the problem of adjusting the grid to satisfy these requirements as best as possible (the choice of temporal and spatial smoothing). Of course this property cannot be used to facilitate the solution of the grid equation viewed as an equation for the positions of the grid points x_i; when explicit expressions for n and R are inserted it merely converts one system of nonlinear equations into another much more complicated one. Its value is rather that it allows general statements to be made about the solutions of the grid equation. For example, if an arbitrary grid equation is used to resolve an asymmetric structure separating two uniform states, there is no guarantee that the asymptotic point concentrations on the left and the right will be equal or related in any simple way. However, with our formulation their ratio will be exactly that of the asymptotic values of R (normally one, but for some applications one might wish to use a "pseudo-Lagrangian" grid and include in R a team proportional to the density). In the same way it is the summability which enables us to place bounds on the spatial and temporal variation of the grid without knowledge of the specific form of R.

3. Tests

We consider first the simple problem of representing the prescribed function,

$$f = \tfrac{1}{2}[1 + \tanh(10^3(x - 0.4))] \exp[-((x - 0.4)/0.2)^2], \tag{12}$$

on the unit interval $[0, 1]$ (tests of this form were an invaluable aid during the development of the grid equation). The hyperbolic tangent with a length scale of 10^{-3} is a good model for a shock smoothed by artificial viscosity; the grid must resolve both this very steep gradient and the smooth variation contributed by the Gaussian term. Because the function is dimensionless and of order unity we can set

both scale functions, F and X to one; thus to resolve the gradients we define the required resolution as

$$R_i = \left(1 + \left(\frac{f_{i+1} - f_i}{x_{i+1} - x_i}\right)^2\right)^{1/2} \tag{13}$$

and the attained resolution as simply

$$n_i = \frac{1}{x_{i+1} - x_i}. \tag{14}$$

Starting with uniformly distributed points we integrate the grid equation forward in time until a stationary distribution is reached. The results with 70 grid points and various values of the parameter α are shown in Figs. 1–3.

On the simple problem the grid equation performs well and exactly as predicted. With the least stiff grid, $\alpha = 2$, we achieve with 70 points a peak resolution equivalent to that of a uniform grid with 10^4 points. The maximum spatial variation of the grid is exactly that specified by the parameter α and the very asymmetric peak in f as a function of x appears on the grid as a symmetric sawtooth in the grid index i. We note also that in the regions on the right and the left, where the function is essentially zero, the asymptotic point concentrations are equal.

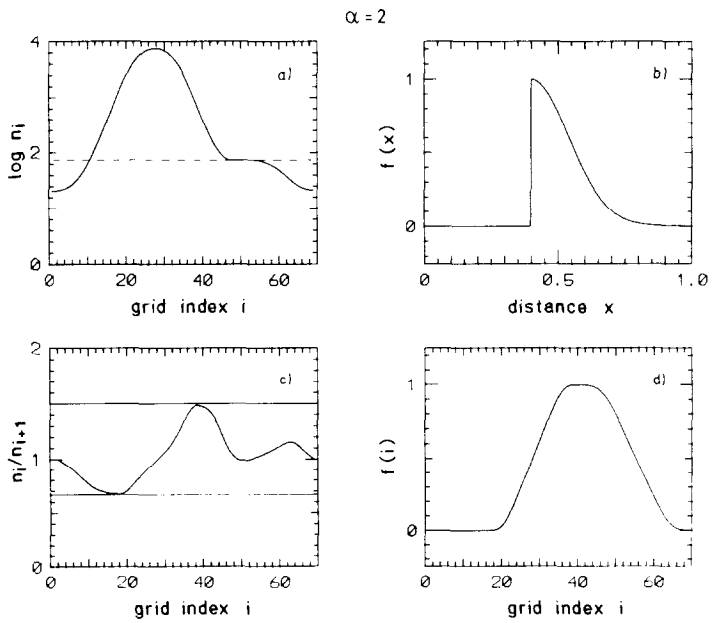

FIG. 1. Distribution of 70 gridpoints for the test function given in Eq. (12) and $\alpha = 2$. (a) Point concentration $\log n_i$ as a function of grid index i. The dashed line corresponds to an equally spaced grid. (b) Test function in physical space. (c) Ratio n_i/n_{i+1} as a function of grid index. The horizontal lines are at $(\alpha+1)/\alpha$ and $\alpha/(\alpha+1)$. (d) Test function in index space.

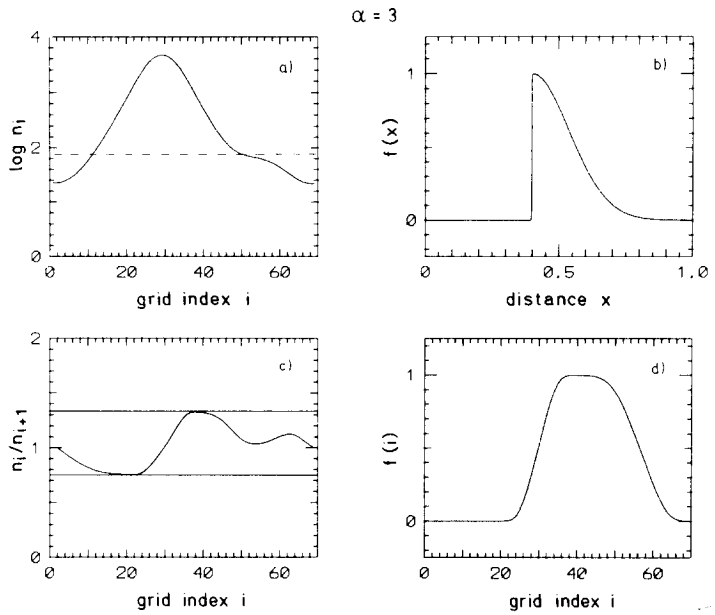

FIG. 2. As Fig. 1 but with $\alpha = 3$.

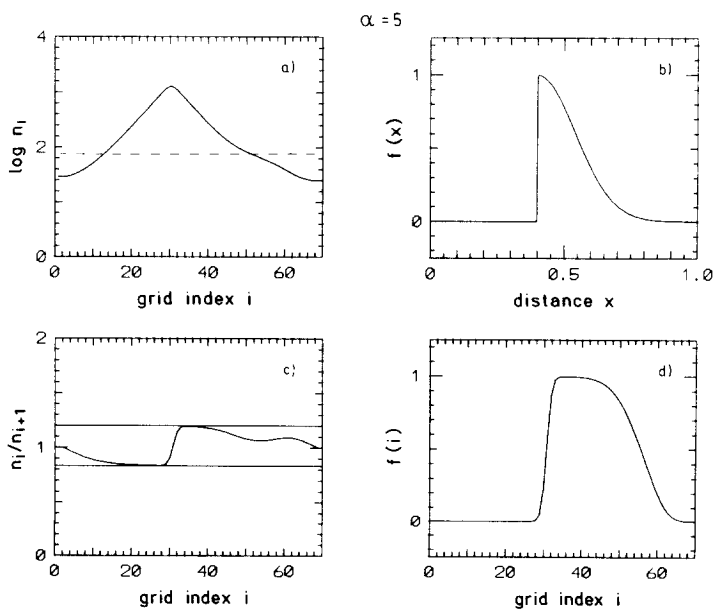

FIG. 3. As Fig. 1 but with $\alpha = 5$.

If the point concentration can only vary from point to point by at most a factor of $1 + 1/\alpha$ it is clear that a local refinement of the grid by 10^m requires at least

$$2m\ln 10/\ln(1 + 1/\alpha) \approx 5\alpha m$$

points (the factor of two comes from the fact that the grid spacing must decrease both on the right and on the left when a steep gradient is resolved). The advantage of adaptive grid methods is immediately obvious; the attainable resolution increases exponentially as the number of points is increased. In our case $m = 3$ so that with $\alpha = 2$ a minimum of about 30 points is required, with $\alpha = 3$ the minimum is 45 and with $\alpha = 5$ at least 75 are needed. Indeed looking at Fig. 3 it is obvious that the grid is starting to suffer from "point exhaustion" (e.g., the left- and right-hand point concentrations are no longer equal) although it is still managing to do quite a creditable job. In this way one can make a quick and crude estimate of the minimum number of grid points needed for any particular problem by summing the minimum number of points required to resolve each smallscale feature.

It should be noted that of this minimum number of points most lie outside the regions where high resolution is required and are there only to provide transition regions in which the point concentration can increase to the value requested. An unfortunate feature of this is that if two smallscale structures requiring similar resolution approach each other, the transition regions between the two features become unnecessary and the points they contain are released as the features merge. If the structures then separate again, or new structures are created, these points

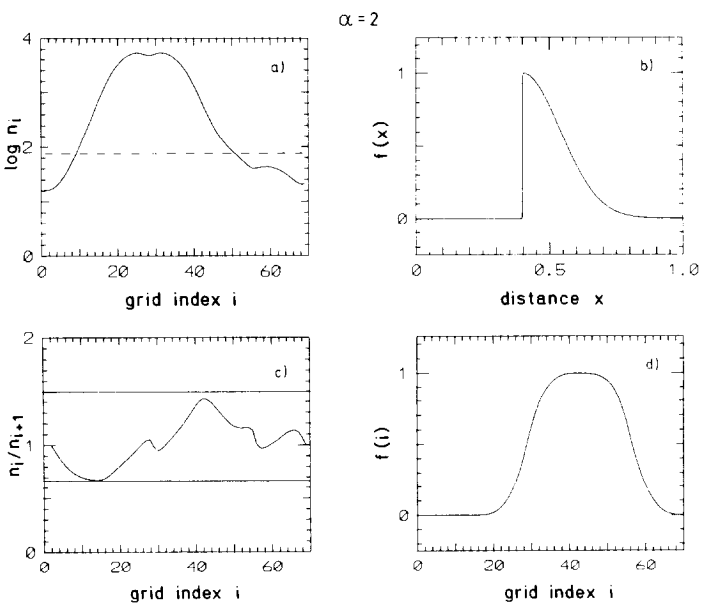

FIG. 4. As Fig. 1 but including second derivatives as specified in Eq. (15).

have to be pulled back in. This can be controlled to some extent by a judicious choice of the grid time constant, but if τ is made too large there will be a loss of resolution in moving features.

If it is necessary to resolve sharp corners as well as steep gradients this is easily achieved. Figure 4 shows the grid obtained by using the definition

$$R = \left(\left(\frac{df}{dx} \right)^2 + \sqrt{\left(\frac{d^2 f}{dx^2} \right)^2 + 1} \right)^{1/2} \tag{15}$$

with the same test function as before. The double square root is based on the idea that if h is the grid spacing, then $h^2(d^2f/dx^2)$ should be uniform across the grid. The spatial discretization of the physical equations will normally have an error $O(h^n f^{(n)})$ for some small integer n; if this error is to be uniformly distributed across the grid we must have $1/h \propto |f^{(n)}|^{1/n}$ in those regions where $|f^{(n)}|$ is large.

4. Method of Solution and Applications

The crucial test of our algorithm is the solution of the hydrodynamic equations (ideal, inviscid) coupled with the grid equation. We use the standard notation of gasdynamics; thus denoting the gas density ρ, velocity $\mathbf{u}$, gas pressure P, internal gas energy density E, we get

$$\frac{\partial \rho}{\partial t} + \nabla \cdot (\rho u) = 0, \tag{16}$$

$$\frac{\partial \rho u}{\partial t} + \nabla \cdot (\rho u u) + \nabla P = 0, \tag{17}$$

$$\frac{\partial E}{\partial t} + \nabla \cdot (E\mathbf{u}) + P \nabla \cdot \mathbf{u} = 0. \tag{18}$$

The internal gas energy density E is related to the gas pressure through an ideal equation of state

$$P = (\gamma - 1)\, E, \tag{19}$$

where γ stands for the adiabatic gas index.

The basic difference is that the structures which should be resolved are not given explicitly through analytic functions; instead they are determined implicitly by the solution of the whole system of equations. The hydrodynamical equations are discretized according to the rules of Winkler, Norman, and Mihalas [18], but we use only a simplified first order version of their difference scheme. For this reason we only resolve gradients in the solution. The discretized system leads to a nonlinear system of algebraic equations which is augumented by the grid equation (11). The coupled system of hydrodynamic and grid equations is solved using a straight

forward Newton–Raphson method. We get basically a blocked pentadiagonal matrix of derivatives which has to be inverted (we refer to standard textbooks or, e.g., to [18] for more details) and usually we need 5 Newton–Raphson iterations to reach the desired relative acuracy of less than 10^{-7}.

We solve two different problems to demonstrate the applicability of this gridpoint distribution technique; in linear geometry we discuss the well-known shock tube problem (see, e.g., Sod [13]) and in spherical geometry we calculate the time evolution of a blast wave with parameters appropriate to a supernova explosion.

a. *Shock Tube Problem*

The shock tube problem starts with a hot, high density, gas (pressure 1.0, density 1.0) in the region $0 \leqslant x \leqslant 0.5$ and a cold, low density, gas (pressure 0.1, density 0.125) in the region $0.5 < x \leqslant 1$. The gas is initially at rest and satisfies an ideal equation of state with $\gamma = \frac{7}{5}$. At $t = 0$ the diaphragm separating the two regions is removed causing a shock wave to propagate into the low density medium and a rarefaction wave into the high density medium. These two flow regions are

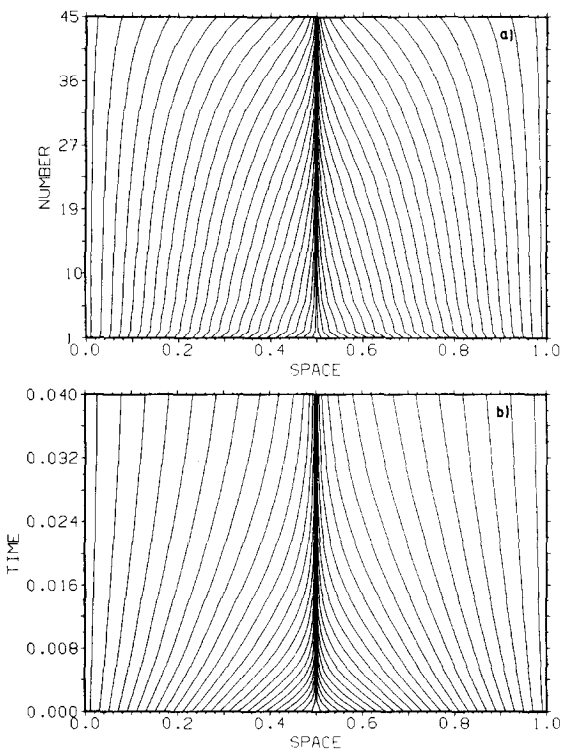

FIG. 5. Gridpoint motion during the creation of the initial grid for the shocktube problem. (a) As a function of time-step number. (b) As a function of "time." The grid relaxes on a time scale $\tau = 10^{-2}$ and is completely relaxed after 4τ.

separated by a contact discontinuity. At $x = 0$ and $x = 1$ we impose reflecting boundary conditions. Analytic solutions have been obtained for the early phases of the evolution by Riemann [12].

This problem exhibits several interactions of nonlinear waves; shock reflection, shock merging, the interaction of a shock with a contact discontinuity and the reflection of a rarefaction wave (for more details see, e.g., Courant and Friedrichs [4]). These can easily be followed on a space-time diagram of the gridpoint motion (see Winkler *et al.* [17] for a more detailed description).

To set up the initial grid distribution we describe here a very simple procedure which takes advantage of the built-in time dependence of the grid equation. Instead of solving the full system of hydrodynamics and grid equation we set $\rho_i = \rho(x_i)$, $u_i = u(x_i)$, and $E_i = E(x_i)$ with the functions $\rho(x)$, $u(x)$, $E(x)$ known from the initial conditions. Keeping these functions fixed we can choose the time parameter $\tau \neq 0$ and start with an initially equidistant grid distribution. We iterate the system until the grid is stationary and this state is usually reached after 50 time steps (Fig. 5). In keeping with the philosophy of finite difference methods using an artificial viscosity we slightly smooth the initial conditions so that discontinuities are approximated by hyperbolic tangents with typical scales of 10^{-3}. This procedure enables us to create an initial grid distribution from any given initial conditions for the physical variables. To clarify we want to state again that the time parameter τ for creating the initial grid is not related to the actual calculation including the physical equations.

Then we start the calculation with the initial grid and the full set of hydrodynamical equations. The parameters in Eq. (3) were $X = 1$, $F_j = 1$, $j = 1, 2, 3$, with f_1 the density, f_2 the velocity, and f_3 the specific internal energy of the gas. Clearly by choosing other scales the performance of the grid equation for specific problems can be optimised, e.g., if good resolution of the velocity structure is important F_2 should be decreased. We use 100 gridpoints, and set the "rigidity" parameter $\alpha = 2$ and the time constant $\tau = 10^{-3}$.

Figures 6–9 depict the variables at $t = 0.01$, $t = 0.23$, $t = 0.32$, $t = 1.0$. The break-up of the initial state into several nonlinear waves and their various interactions can be seen. The rounded edges of the rarefaction wave are probably a consequence of the low-order discretization in space and time. The discontinuities are represented in a quite satisfactory way. A useful side effect of these test calculations is that we can put "error-bars" on the numerical solutions: the calculated solution agrees with the analytic solution to better than 1%. The reflection of the flow on the walls generates one additional numerical error. This so-called wall heating causes an unphysical entropy spike, which affects only some cells located at the wall. The expanding grid tends to correct this by mixing material with the correct entropy to the tiny fraction of overheated gas although in calculations with a large number of points and a small scale for the internal energy the feature remains (cf. Winkler *et al.* [17, 18]).

Figure 10 shows the space-time evolution of the gridpoints. We plot every second point. The point concentrations associated with the shock and the contact discon-

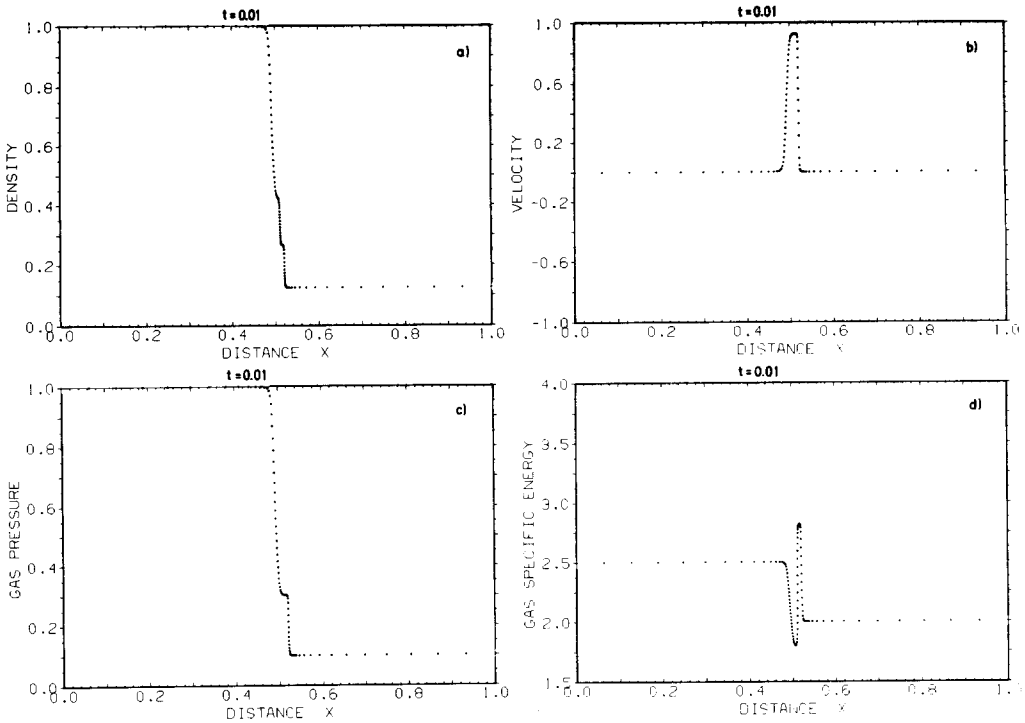

FIG. 6. The shocktube results at $t = 0.01$.

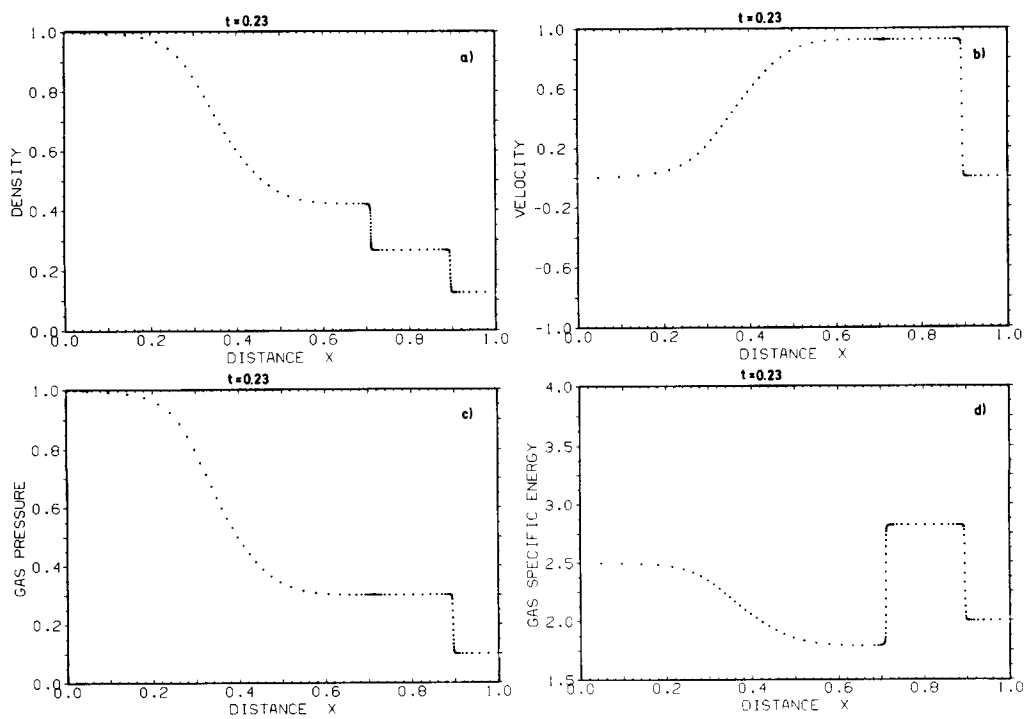

FIG. 7. The shocktube results at $t = 0.23$.

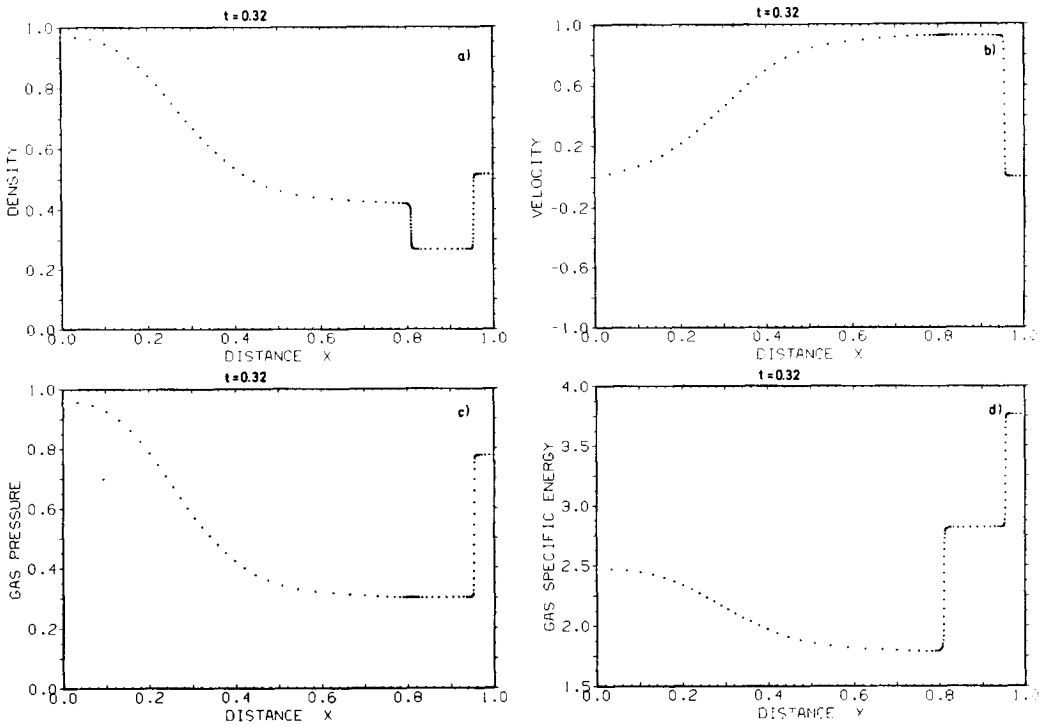

FIG. 8. The shocktube results at $t = 0.32$.

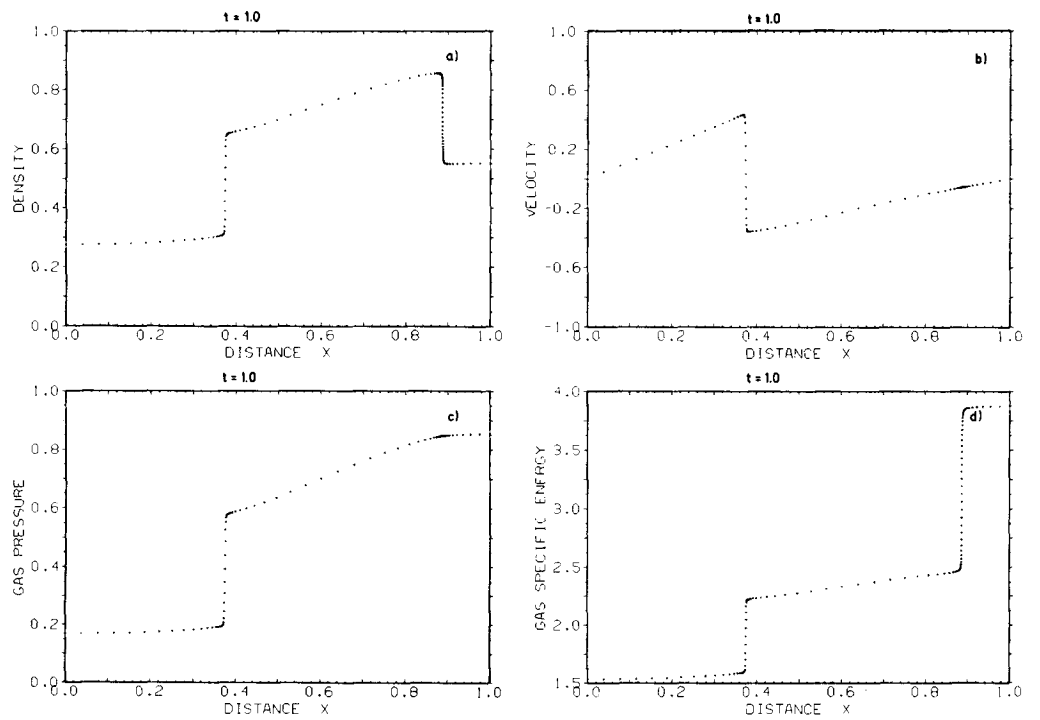

FIG. 9. The shocktube results at $t = 1.0$.

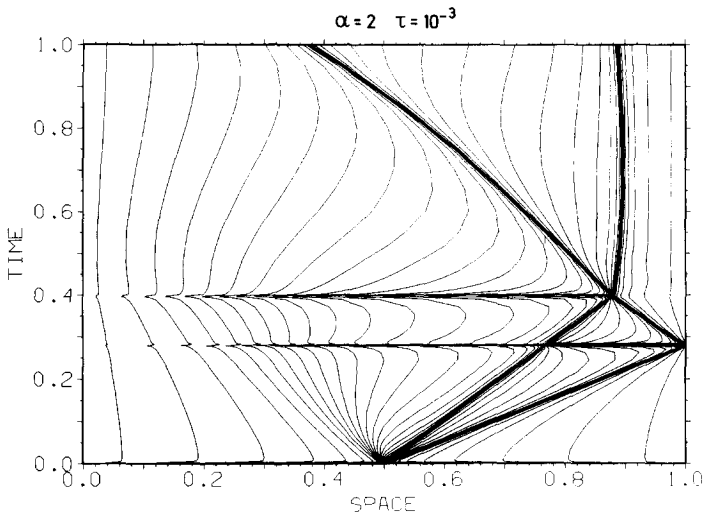

FIG. 10. The gridpoint motion during the shocktube calculation. Every second gridpoint is plotted. The dark lines correspond to the motion of the shock and the contact discontinuity, respectively. At $t \approx 0.28$ the shock is reflected at the right wall and at $t \approx 0.41$ the shock interacts with the contact discontinuity.

tinuity are obvious while the expansion wave, though not so pronounced, can also be seen. At $t \approx 0.28$ the shock reflects from the wall ($x = 1$). The gridpoints are pulled out to resolve the remaining structures. This motion is controlled by the time scale parameter $\tau = 10^{-3}$. After the shock reflection the gridpoints are pulled in again causing a horizontal black line on the plot. The same holds for the interaction of the contact discontinuity with the shock ($t \approx 0.41$) because now only one locally refined grid region is needed to resolve the two steep gradients. Since we have not encountered any problems during these phases, we do not incorporate an asymmetric time-filtering as advocated by Winkler *et al.* [18]. The whole evolution requires about 100 time steps. On the comoving grid the solution looks almost stationary allowing the implicit method to take rather large time steps; typical Courant-numbers are in the range 10^{2-3}.

b. *Spherical Blast Wave*

To demonstrate the broad applicability of the adaptive grid technique we now solve a problem in spherical geometry where we have to cover many orders of magnitude variation in both dependent and independent variables; a "standard" supernova exploding in the hot phase of the interstellar medium [10]. For the progenitor star we use a very simple model of a red giant star; the density is taken to be constant at 10^{-11} g cm^{-3} out to 5×10^{14} cm and then to decrease exponentially with a length scale of 10^{14} cm until the density of the external medium is reached. We assume initial pressure equilibrium and then deposit $E_{SN} = 10^{51}$ erg uniformly as thermal energy within a radius of 10^{13} cm. The exact details of this

model are probably not critical for the subsequent evolution, the important parameters are the explosion energy E_{SN} and the ejecta mass of five solar masses. The external medium is a tenuous low density gas at rest with density $\rho_{ext} = 5 \cdot 10^{-27}$ g cm^{-3} at a temperature $T_{ext} = 5 \cdot 10^5$ °K.

We use the hydrodynamic equations written in conservative form for spherical geometry. The discretization is unchanged and corresponds basically to the linear case, but we use a tensor formulation of the artificial viscosity [14] and take as a typical length scale for broadening the shock front 10^{-3} of the local shock radius. We also include a small amount of heat conduction ($\sigma = 10^{-17}$ cm^2 sec^{-1}) to restrict the thickness of the propagating contact discontinuity (see again Winkler *et al.* [18] for more details on the actual discretization).

The main difference in the grid equation is the use of logarithmic scaling, i.e., $X = x$ and $F_j = f_j$. These scales can be discretized in several ways; for this rather extreme problem we found it necessary to discretize F_j as

$$\frac{1}{F_{j,i}} = \frac{1}{2}\left(\frac{1}{f_{j,i+1}} + \frac{1}{f_{j,i}}\right).$$

The use of a harmonic mean instead of the rather more natural arithmetic mean prevents the grid from "tearing" (W. M. Tscharnuter, Personal communication). If the arithmetic mean were used the dimensionless gradient, $(f_{j,i+1} - f_{j,i})/(f_{j,i+1} + f_{j,i})$, would be bounded (for positive f) between plus and minus one, thus if the number of points in a near-discontinuity becomes small this form "saturates" and is no longer a good measure of the desired resolution. The grid then tends to concentrate all the variation in one cell. The harmonic mean essentially avoids this problem by making the gradient dimensionless with respect to the smaller of the left and right values. The arithmetic mean can be used for X, i.e.,

$$X_i = \tfrac{1}{2}(x_i + x_{i+1}).$$

We use $j = 1, 2$ with f_1 the density and f_2 the specific internal energy. The time constant is set to zero, i.e., $\tau = 0$ so that the gridpoints react immediatly to changes in the physical variables. The spatial smoothing corresponds to $\alpha = 2$ and we use 400 gridpoints.

The early phases of the supernova evolution are shown in Fig. 11. The stored thermal energy causes a strong shock to run through the extended envelope of the

$t = 10^3$, 10^4, 10^5 sec. At $t = 10^6$ sec the shock accelerates again down the large density gradient which represents the stellar atmosphere. The fourth curve $t = 2 \cdot 10^6$ sec shows the shock in the atmosphere. The shock speed approaches the speed of light and we cannot draw detailed conclusions during this phase since we use only the Newtonian limit of the hydrodynamical equations. In any case, we do not try to simulate a "realistic" supernova explosion, but we consider this to be a very challenging test problem for our grid equation. From $t = 3 \times 10^6$ sec up to $t = 5 \times 10^{11}$ sec the further evolution is characterized by a free expansion with the

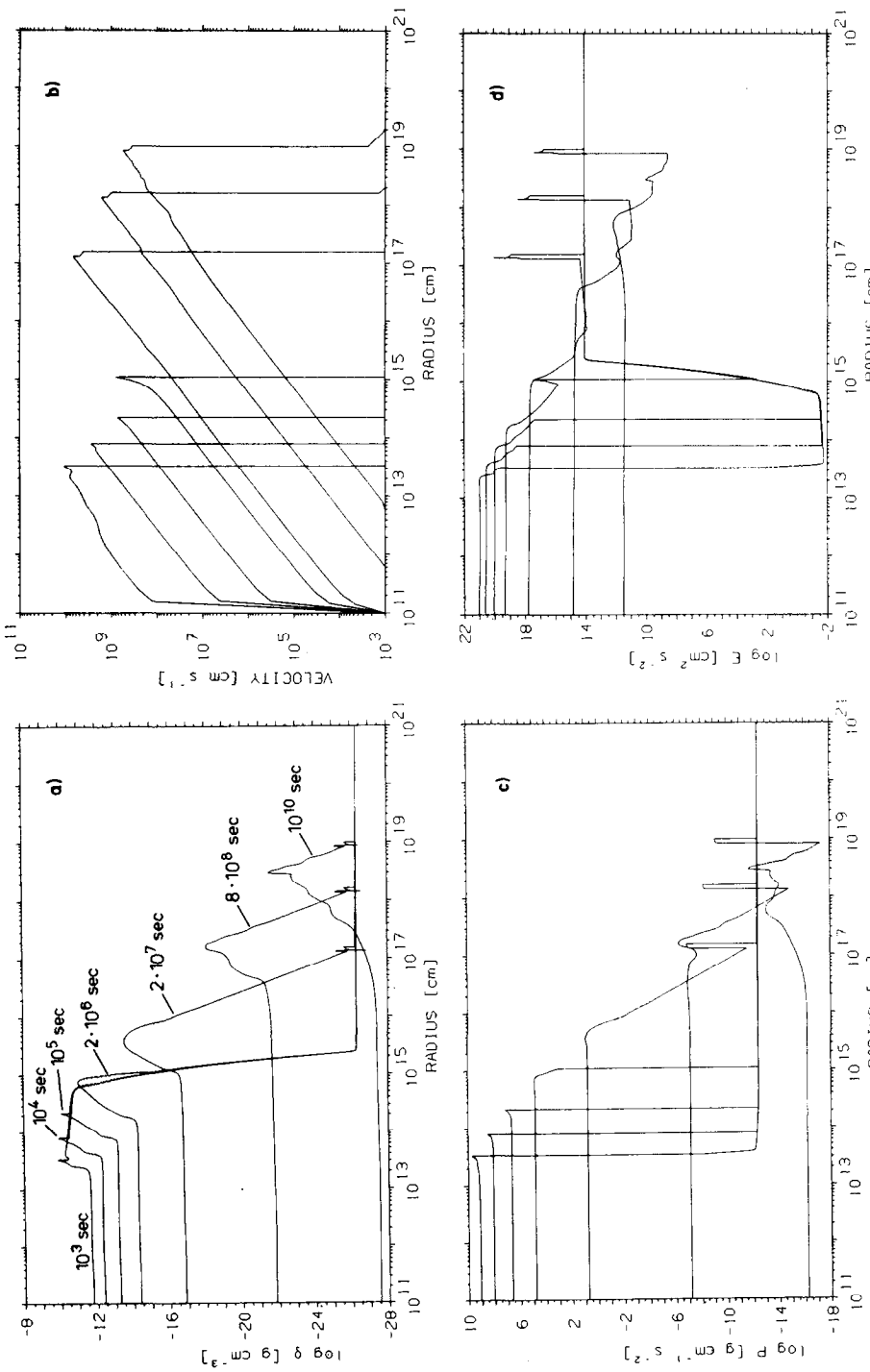

FIG. 11. The early phases of a supernova explosion are displayed at times $t = 10^3$, 10^4, 10^5, 2×10^6, 2×10^7, 8×10^8, 10^{10} sec. The first three curves show the motion of the strong shock wave in the stellar interior, the fourth curve depicts the phase where the shock runs through the stellar atmosphere and the last three correspond to the free expansion phase in the interstellar medium.

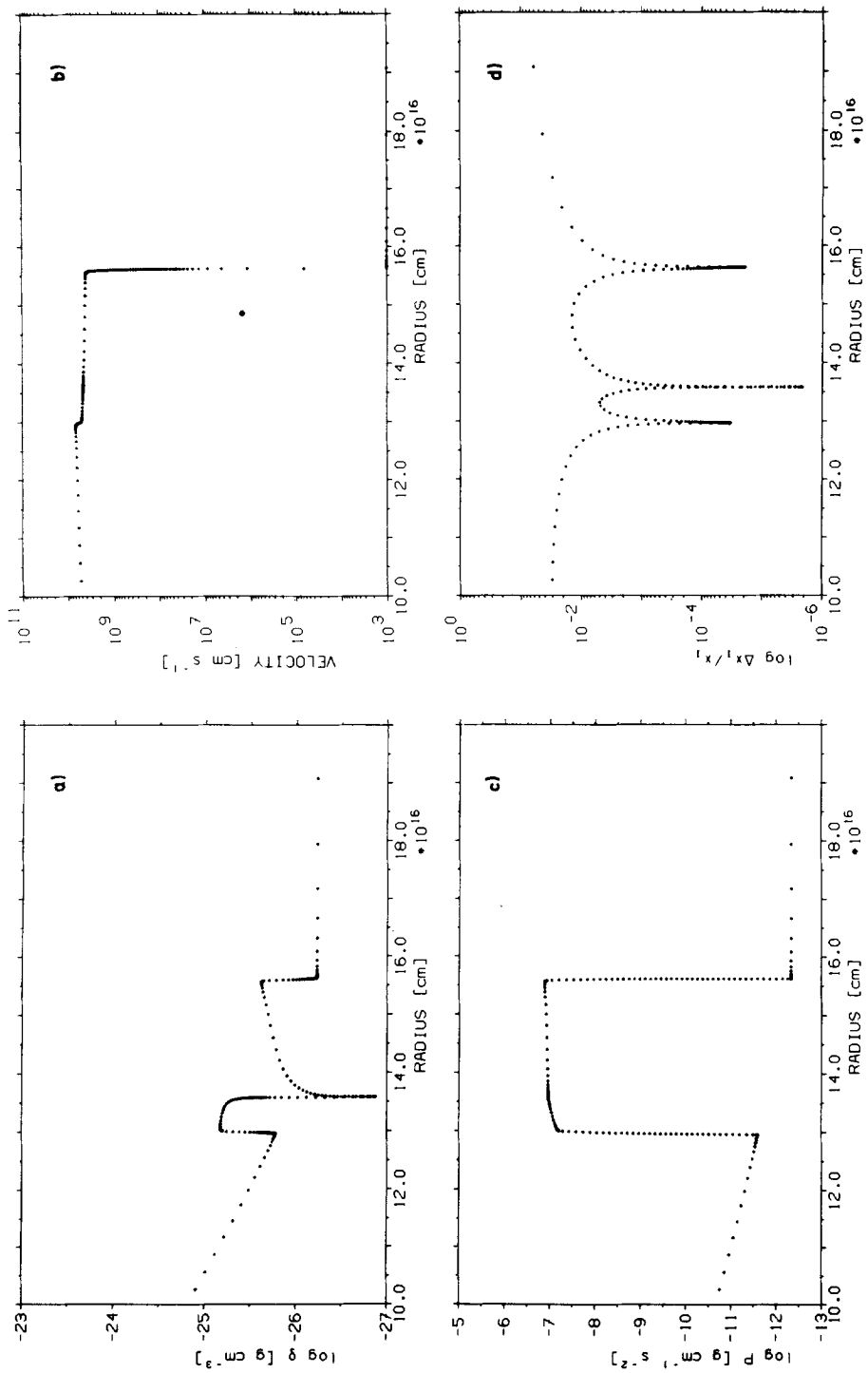

FIG. 12. The contact discontinuity and double shock structure at $t = 2 \times 10^7$ sec. To emphasise the resolution achieved using the adaptive grid the individual gridpoint values are plotted between 10^{17} and 2×10^{17} cm. The relative grid spacing is shown in (d), at the discontinuities the resolution equals that of a uniform grid with 10^{4-6} points.

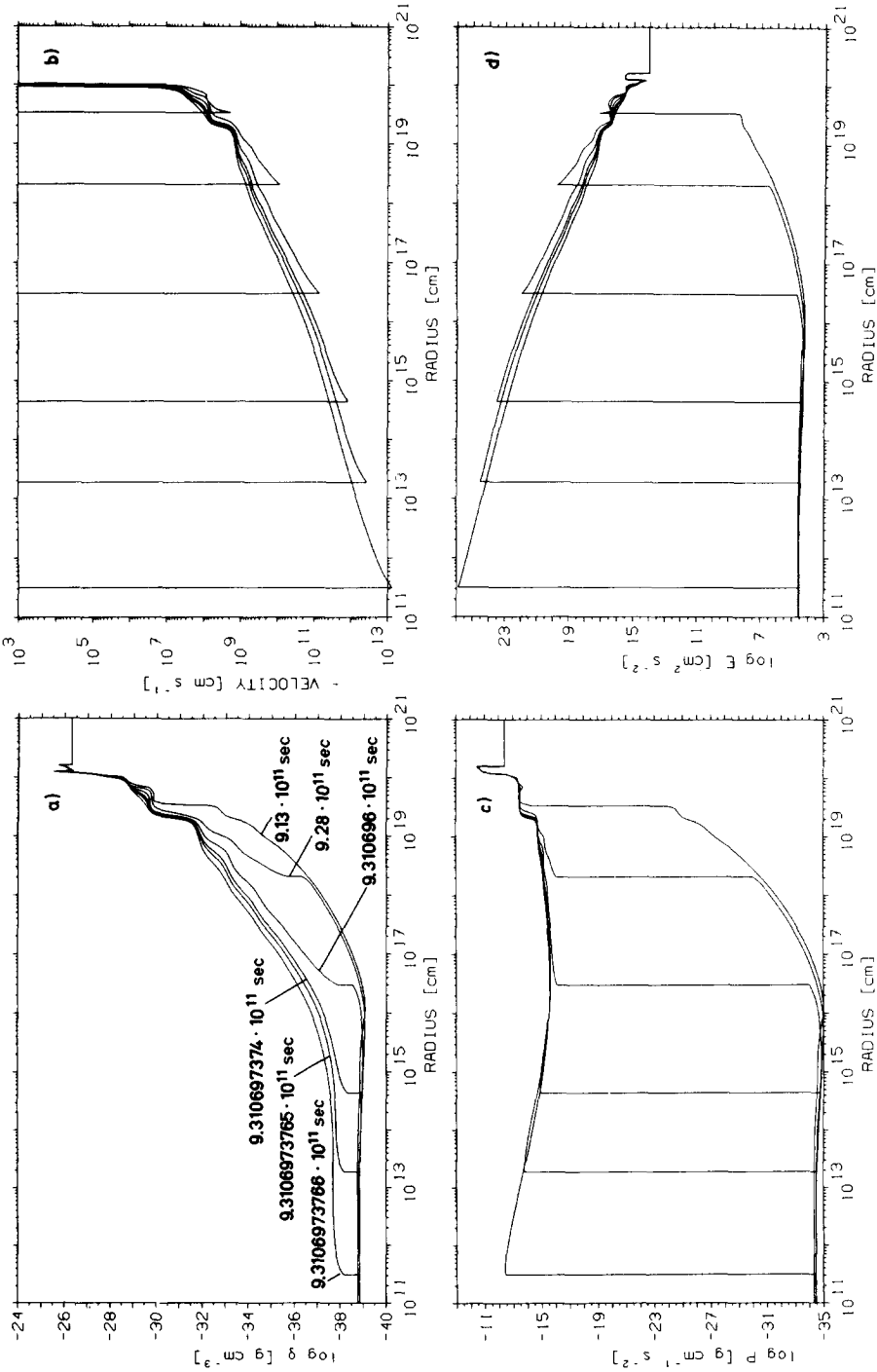

FIG. 13. The supernova results a $t = 9.13 \times 10^{11}$, 9.28×10^{11}, 9.310696×10^{11}, $9.310697374 \times 10^{11}$, $9.3106973765 \times 10^{11}$, $9.3106973766 \times 10^{11}$ sec, showing the propagation of the reverse shock into the interior. Inside 10^{15} cm the reverse shock is travelling so fast that it reaches the center in a few thousand seconds.

following typical structure: the ejecta are separated from the external medium by a contact discontinuity bounded by two shocks. The interior cools down adiabatically and the kinetic energy of the explosion is transformed to thermal energy in the two shocks. The reverse shock is advected with the fluid, but moves backward relative to the contact discontinuity. The strong forward shock compresses the interstellar material. These can be seen in Fig. 11 and in more detail in Fig. 12 where we have plotted every gridpoint.

At about 5×10^{11} sec the swept-up mass becomes comparable to the ejecta mass and the reverse shock runs inwards and heats the interior. This phase is shown in Fig. 13. The extremely low interior densities lead to very high shock velocities (1000 times the velocity of light!). At a radius of 10^{11} cm we impose a reflecting boundary condition. When the shock reaches this inner radius a disturbance propagates back up the density gradient, interacts with the contact discontinuity and a second

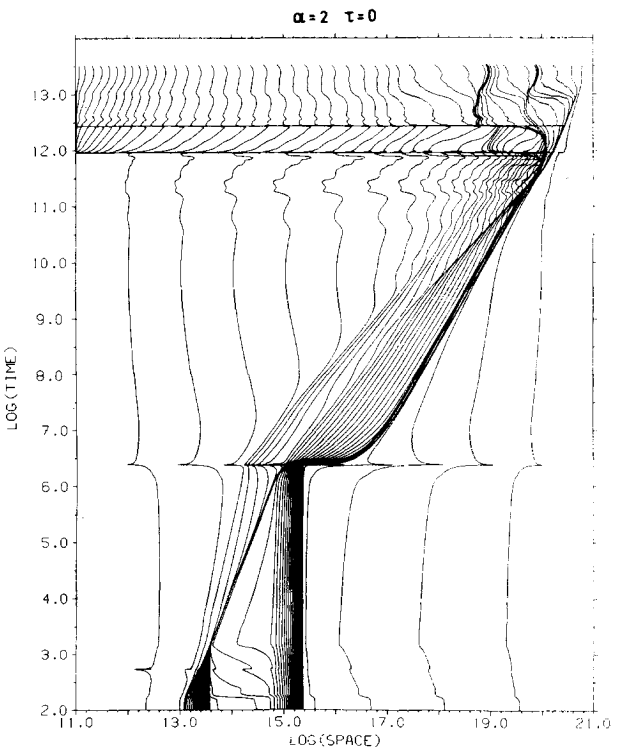

FIG. 14. The gridpoint motion during the supernova calculation. Every 8th gridpoint is plotted. The initial point concentrations at $R = 10^{13}$ cm resulting from the strong gradient in the thermal energy deposition and at $R = 5 \times 10^{14}$ cm resulting from the density gradient in the stellar atmosphere are clearly seen. At $t = 2 \times 10^{7}$ sec the shock runs through the stellar atmosphere and speeds up to a high velocity. At $t = 9 \times 10^{11}$ sec the reverse shock starts travelling inwards and at $t = 2.7 \times 10^{12}$ sec a second somewhat weaker reverse shock runs into the interior. These two events are indicated by the horizontal motion of the gridpoints. The calculation was stopped when the Mach-number of the outermost shock decreased to unity at $t = 3.4 \times 10^{13}$ sec.

reverse shock forms. After this the interior is almost in pressure equilibrium although small disturbances remain. The internal pressure is close to the external pressure so that no Sedov-phase occurs.

Figure 14 shows the complete gridpoint evolution for this calculation. The entire calculation ran without manual intervention and without carefully chosen parameters. It required about 4000 time steps and took 40 min on a CRAY-1 computer. The smallest timestep was 10^{-12} sec and the largest 10^{11} sec. The maximum point concentration was 10^9.

Concluding Remarks

The two solutions exhibited in the last section demonstrate that the use of Simple Adaptive Grid Equations (our favourite acronym is SAGE) constitutes a valuable technique for the numerical solution of evolution equations in one spatial dimension. An extension of the method to multidimensional problems would appear to be possible by defining R and n as tensors. However this must await the further development of multidimensional implicit finite difference methods and it may be that grid refinement methods [1] are better in more than one dimension.

Acknowledgments

We are grateful to W. M. Tscharnuter for many discussions of the desirable features of a grid equation. In developing this approach to the problem we tested a large number of ideas, most of them more complicated than the final solution. The labour involved would have been prohibitive without the help of the REDUCE system [9] which calculated the many derivatives needed.

References

1. M. J. Berger and J. Oliger, *J. Comput. Phys.* **53**, 484 (1984).
2. J. U. Brackbill and J. S. Saltzman, *J. Comput. Phys.* **46**, 342 (1982).
3. R. Courant, K. O. Friedrichs, and H. Lewy, *Math. Ann.* **100**, 32 (1928).
4. R. Courant and K. O. Friedrichs, *Supersonic Flows and Shock Waves* (Interscience, New York, 1948).
5. S. F. Davis and J. E. Flaherty, *SIAM J. Sci. Stat. Comput.* **3**, 6 (1982).
6. H. A. Dwyer, R. J. Kee, and B. R. Sanders, *AIAA J.* **18**, 1205 (1980).
7. H. A. Dwyer and O. O. Onyejekwe, in *Proceedings, 9th Int. Conf. on Numer. Meth. in Fluid Dynamics*, (Lecture Notes in Physics, No. 218 (Springer–Verlag, Berlin, 1985).
8. R. J. Gelinas and S. K. Doss, *J. Comput. Phys.* **40**, 202 (1981).
9. A. C. Hearn, *REDUCE User's Manual*, Univ. of Utah Report No. UCP-19, 1973 (unpublished).
10. C. F. McKee and J. P. Ostriker, *Ap. J.* **218**, 148 (1977).
11. E. V. Paleologou and T. Ch. Mouschovias, *Ap. J.* **275**, 833 (1983).
12. B. Riemann, *Gesammelte Werke* (2. *Auflage*) (Teubner, Leipzig, 1892), p. 159.

13. G. A. SOD, *J. Comput. Phys.* **27**, 1 (1978).
14. W. M. TSCHARNUTER AND K.-H. A. WINKLER, *Comput. Phys. Comm.* **18**, 171 (1979).
15. A. B. WHITE, *SIAM J. Numer. Anal.* **19**, 683 (1982).
16. K.-H. A. WINKLER, Ph. D. thesis, Univ. of Göttingen, 1976 (unpublished).
17. K.-H. A. WINKLER, M. L. NORMAN, AND M. J. NEWMAN, *Physica D* **12**, 408 (1984).
18. K.-H. A. WINKLER, M. L. NORMAN, AND D. MIHALAS, preprint MPI für Astrophysik Garching, MPA-112, 1984, Comput. Techniques Series, submitted.